



Cite this: *J. Mater. Chem. B*, 2018,
6, 1373

Size-controlled, colloidally stable and functional nanoparticles based on the molecular assembly of green tea polyphenols and keratins for cancer therapy†

Zeng Yi, Zhe Sun, Guangcan Chen, Huaiying Zhang, Xiaomin Ma, Wen Su, Xinxing Cui and Xudong Li *^{ID}

While intelligent nanoparticles with therapeutic effects provide a resolving strategy for low drug loading efficacy, poor metabolism and elimination of current nanoparticulate drug delivery systems, precise preparation of colloidally stable but stimuli-responsive nanocarriers with size tunability is still a challenging task. Here, we develop a facile and sustainable method through the use of naturally reproducible green tea polyphenols and hair keratins to prepare biocompatible, colloidally stable, stimuli-responsive nanoparticles with therapeutic effects. The present strategy simply involves covalent interactions of tea catechins and keratins, giving rise to the molecular assembly of size-controlled nanoparticles (30–230 nm) which are long-term colloidally stable at physiological media but are disassembled under pathological conditions, ideally for targeted delivery of anticancer drugs. The cell experiments confirmed that these nanoparticles are bio-safe, have the inherent bioactivity of tea catechins, and that the drug-loaded nanoparticles yield a higher cancer cell inhibition rate than free drugs. In addition, the nanoparticles are found to improve the bioavailability of tea polyphenols, according to animal studies, which further demonstrates that the use of nanoparticles as drug carriers results in enhanced anticancer efficacy with negligible systemic toxicity. Given that large-scale preparation of size-controlled nanoparticles could already be easily achieved, the present study actually provides an innovative nanotechnological approach to make good use of green tea polyphenols with beneficial health effects, potentially for therapeutic and preventive purposes.

Received 22nd December 2017,
Accepted 29th January 2018

DOI: 10.1039/c7tb03293e

rsc.li/materials-b

1. Introduction

Precise preparation of nanoparticles (NPs) is of paramount importance for diagnosis, treatment and prevention of many diseases.^{1–3} NPs play pivotal roles in nanoparticulate pharmaceutical drug delivery systems (NDDSS) in order to overcome the inadequacies of many chemotherapeutic drugs, such as the poor bioavailability, unfavorable pharmacokinetics and irreversible toxic side effects.⁴ Ideal NDDSS are designed to be colloidally stable but to stimuli-responsively disassemble at intended sites, thus securing no leakage of agents during circulation in the blood before targeted delivery,⁵ via enhanced permeability and retention (EPR) effects or via ligand-mediated specific targeting, and release of agents sensitive to pathological environments such as abnormal pH, temperature, enzyme and redox conditions.⁶

National Engineering Research Center for Biomaterials, Sichuan University, Chengdu 610064, P. R. China. E-mail: xli20004@yahoo.com;
Fax: +86 (0)28 8541 2102; Tel: +86 (0)28 8541 2102

† Electronic supplementary information (ESI) available: Main parameters, human hair keratin extraction, SDS-PAGE and SEM and TEM images, etc. See DOI: 10.1039/c7tb03293e

Carriers of NPs with therapeutic effects are further highly acclaimed because of the safety concerns of carriers such as poor metabolism and elimination, which may compromise the value of their use.^{7,8} In addition, the size of the NPs is a principal determinant for their biological performance, and many studies suggested that size had a direct correlation with their extravasation, systemic distribution, cellular targeting and internalization.^{9–11} Therefore, the rational design and facile preparation of such functional nanoparticles with precisely tunable sizes are receiving extensive attention, but still remains a great challenge.¹² So far, most of the NDDSS are derived from a non-renewable petrochemical feedstock, but the strategies based on the use of naturally reproducible and even edible products are emerging.¹³

Tea catechins are a group of polyphenolic compounds extracted from green tea leaves, having a three-membered flavan ring structure of A-, B- and C-rings with or without a galloyl group¹⁴ (Fig. 1). Owing to the activity of their vicinal di- or tri-hydroxy groups, catechins (Cat), especially epigallocatechin-3-gallate (EGCG), are known to have preventive and therapeutic effects against cancer and many other diseases.¹⁵ Nowadays, nanotechnology has been intensively used to tackle obstacles associated with the

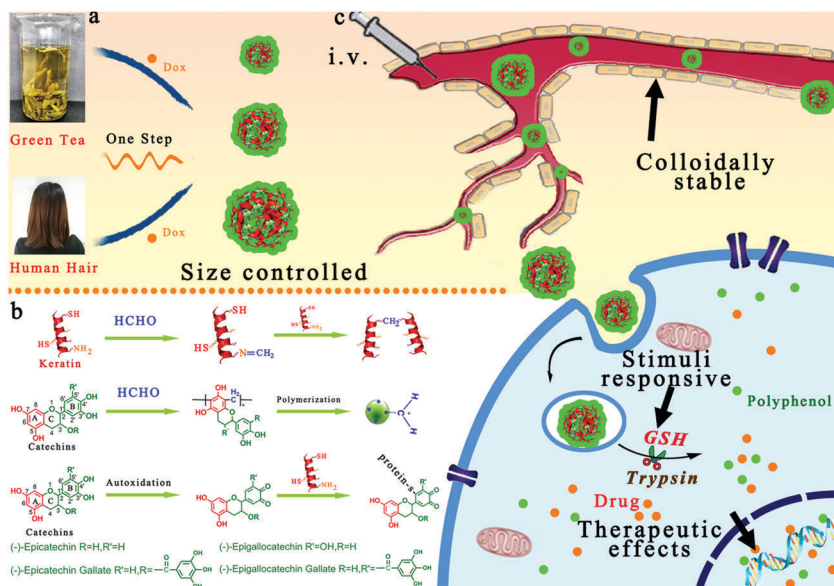


Fig. 1 Schematic illustration of (a) a simple and sustainable strategy for fabricating catechin-based functional nanospheres from human hair keratins and green tea polyphenols, (b) molecular interactions of nanosphere assembly, and (c) administration of these colloidally stable, GSH and enzyme dual stimuli-responsive nanoparticles with therapeutic effects for enhanced cancer therapy.

use of catechins, such as rapid metabolism, inefficient systemic delivery and poor bioavailability of catechins.¹⁶ The encapsulation of tea catechins (Cat) within capsule spheres or the formation of Cat-based complexes with biomacromolecules is reported to enhance the bioavailability and therapeutic efficacy of tea polyphenols (TPs).^{17,18} In addition, EGCG directly exhibits the capabilities to enhance the anticancer capacities of a small molecule or protein drugs and at the same time, to reduce the side effects, *e.g.*, alleviating the cardiotoxicity of doxorubicin (DOX).¹⁹ These biomedical findings of both EGCG and oligomeric EGCG (OEGCG),^{20–23} along with the emerging self-assembly of functional tea catechins,^{24,25} further promote the incorporation of TP into carriers for the delivery of chemotherapeutic agents. Recently, pure TP nanoparticles were used solely as carriers of DOX, achieving enhanced anticancer efficacy with negligible systemic toxicity.²⁶ To the best of our knowledge, the size-controlled preparation of TP-based nanoparticles with colloidally stable but stimuli-responsive properties has not yet been reported. Proteins such as silk fibroin,²⁷ BSA²⁸ and keratin are great candidates for delivering drugs or other bioactive substances *in vivo*. Keratins are a group of cysteine-rich fibrous proteins present in filamentous or hard structures such as hairs, wools, *etc.*²⁹ Extracted from human hair fibers, keratin proteins are widely used as a new generation of smart biomaterials for various medical purposes including the repair and regeneration of defected tissues and the intelligent delivery of anticancer drugs.^{30,31}

In the present work, we report a one-pot precise preparation method for size-controlled, colloidally stable and functional nanoparticles with naturally reproducible green tea polyphenols and keratin proteins (Fig. 1a). The present strategy primarily involves the covalent assembly of catechins and keratins in the presence of formaldehyde in water in an ambient environment. As shown in the schematic in Fig. 1b, formaldehyde reacts with

the amino and thiol groups of the amino acids of keratins, yielding methylol derivatives. These methylol groups can be dehydrated to form an imine, *i.e.*, a schiff-base.³² The imine is prone to react with several nucleophilic amino acid residues, leading to the formation of methylene bridges in keratins. The reaction between formaldehyde and catechins is an aldol condensation-type reaction, and comprises methylolation, condensation and polymerization, yielding oligomeric catechins with methylene bridges.³³ In addition, the direct covalent binding of keratins to catechins also occurs, including methylene bridging of catechins and keratins and covalent thiol-flavonoid adducts.³⁴ The latter are formed by the electrophilic reaction of the thiol groups of keratins with polyphenol quinone, a highly reactive intermediate in the autoxidation of catechol-type or pyrogallol-type catechins. The aforementioned reactions jointly contribute to initiating the molecular assembly of size-controlled, functional catechin-keratin nanoparticles, simply by changing different concentration combinations of keratin, catechin and formaldehyde in the feedstock. We further demonstrate that these nanoparticles, incorporating the salient features from naturally reproducible tea polyphenols and keratin proteins, are colloidally stable under physiological conditions but disassemble under pathological conditions, and have therapeutic effects, ideally as drug carriers to overcome the distinct biological barriers resulting in enhanced anticancer efficacy with negligible systemic toxicity (Fig. 1c).

2. Experimental section

2.1 Materials

Formaldehyde, chloroform, methanol, Tris-HCl, thiourea, urea, 2-mercaptoethanol and ethyl alcohol were purchased from Kelun

pharmacy company (Chengdu, China). Doxorubicin hydrochloride (DOX) was purchased from Meilun Biological technology (Dalian, China). Cell counting kit-8 (CCK-8) was purchased from Dojindo Laboratories (Japan). Catechin powder (EGCG wt% \geq 80%) was purchased from Wuxi Taiyo Green Power Co. Ltd. (Jiangsu, China). Folin-Ciocalteu's phenol reagent was purchased from Beijing Solarbio Science & Technology (Beijing, China). Sodium hydrogen carbonate was purchased from Ke Long (Chengdu, China). Roswell Park Memorial Institute 1640 medium (RPMI-1640) and fetal bovine serum (FBS) were purchased from Gibco (USA). Penicillin-streptomycin solution was purchased from Hyclone (USA).

2.2 Preparation of nanoparticles

With different concentration combinations of catechin, keratin and formaldehyde, nanoparticles of np-1–np-9 were obtained together with three controls kf-0, kc-0 and cf-0. The main parameters are summarized in Table S1 (ESI[†]). In a typical synthesis of np-4 particles, 50 mL of keratin solution (0.2 mg mL^{-1}) was mixed with 50 mL of TP solution (10 mg mL^{-1}). Then, 0.81 mL of an aqueous solution of formaldehyde (37%) was added to the prepared mixture to initiate the molecular assembly of the nanoparticles. After stirring for 24 hours at room temperature, the products were collected by centrifugation, washed with water three times, and finally were lyophilized or re-dispersed in water at $4\text{ }^\circ\text{C}$ for subsequent characterization and experiments.

2.3 Characterization

Microscopy. The morphology of the samples was observed using a Hitachi S-4800 and JSM-7500F scanning electron microscope (SEM). Transmission electron microscopic (TEM) images were obtained using a JEOL JEM-1200 EX microscope operating at 120 kV. For TEM observations, the appropriate nanoparticle sample was put in a 1.5 mL centrifuge tube and after being diluted with water, $\sim 5\text{ }\mu\text{L}$ of the sample was dipped onto a glow-discharged formvar/carbon-coated copper grid (Electron Microscopy Sciences), followed by staining with 1% phosphotungstic acid.

UV-vis. By forming a suspension in water, the luminescence properties of the samples were measured using ultraviolet-visible (UV-vis) spectroscopy. The UV spectroscopy was undertaken using a Persee TU-1901 UV/Vis spectrophotometer.

FT-IR. For FT-IR analysis, the nanoparticle solutions were lyophilized. The powders were dispersed in potassium bromide (KBr) and compressed into disks. To obtain all the FT-IR spectra, we performed 32 scans over the range of $400\text{--}4000\text{ cm}^{-1}$.

NMR. For $^1\text{H-NMR}$ analysis, the lyophilized nanoparticles were dissolved in DMSO-D₆. ^1H NMR spectra of the nanoparticles were recorded on a Bruker Avance II NMR spectrometer at 400 MHz.

Dynamic light scattering (DLS). Nanoparticle size, polydispersity index and surface charge were determined through dynamic light scattering analysis using a Nanosizer ZS (Malvern Instruments). To investigate the interaction in the catechin-keratin nanoparticles, different concentrations of sodium

dodecyl sulphate (SDS) and urea were added to the nanoparticle suspensions, and after 2 h of incubation the diameters of the nanoparticles were measured using DLS.

High performance liquid chromatography (HPLC). HPLC was used to determine the residual formaldehyde content in the nanoparticles. 20 mg of lyophilized np-4 nanoparticles were dispersed in 5 mL of acetonitrile and ultrasonicated for 20 min. 2.5 mL of 2,4 DNPH (6 mg mL^{-1}) was added to the np-4 acetonitrile solution (4 mg mL^{-1}) and mixed well. The samples were incubated at $40\text{ }^\circ\text{C}$ for 60 min in a 10 mL EP tube. Formaldehyde was quantitatively converted to its Schiff base in 60 min. After incubation, the solution was collected, membrane filtered ($0.2\text{ }\mu\text{m}$) and analyzed using HPLC. Analyses were performed on a C18 column ($150 \times 4.6\text{ mm}$) using HPLC (Agilent HPLC System, USA) coupled to a UV-vis detector. The wavelength was set to 355 nm and the oven temperature at $30\text{ }^\circ\text{C}$. The HPLC operated as isocratic elution with a mixture of water/methanol ($35:65$, v/v); flow rate at 1.0 mL min^{-1} . The total run time was 8 min. 10 mg L^{-1} and 20 mg L^{-1} standard samples of formaldehyde were used as references.

2.4 Catechins content

The Folin-Ciocalteu method was used to determine the content of catechins. 1 mL of the np-4 suspension was mixed with 5 mL of 10% Folin-Ciocalteu reagents for 3–8 minutes, then 4 mL of 7.5% sodium carbonate solution was added, after incubation for 1 h in the dark, the absorbance was measured at 765 nm. The different concentrations of catechin solutions determined by Folin-Ciocalteu colorimetry were used as the calibration curves. In this study, the productivity of the nanoparticles was calculated using the formula: productivity = (catechins in nanoparticles)/(the content of initial catechins) $\times 100\%$.

2.5 Drug loading experiments

For the preparation of DOX/np-4, 10 mL of np-4 (2 mg mL^{-1}) was added into a brown bottle and mixed with 10 mL of DOX (2 mg mL^{-1}). The mixture was stirred at $4\text{ }^\circ\text{C}$ for 24 h, DOX was encapsulated into np-4, then the mixture was centrifuged at $15\,000\text{g}$ for 20 min at $4\text{ }^\circ\text{C}$. The drug loading capacity was about 16.7% ($n = 3$). The amount of DOX encapsulated in DOX/np-4 was examined using a UV-vis spectrophotometer with an absorption wavelength of 480 nm in DMSO. A standard curve of doxorubicin was established in the range of $10\text{--}100\text{ }\mu\text{g mL}^{-1}$.

2.6 Stimuli response of np-4 and DOX release from the nanoparticles

To investigate the stimuli-sensitivities, np-4 suspensions ($200\text{ }\mu\text{g mL}^{-1}$) were incubated under different biomimetic conditions of $10\text{ }\mu\text{M GSH}$, 2 mM GSH , 5 mM GSH , 10 mM GSH with 0.04 mM trypsin individually. The size change of np-4 was determined via dynamic light scattering (DLS). *In vitro* DOX release was carried out in a series of HEPES buffers (pH 7.4, 10 mM GSH and $10\text{ mM GSH} + 0.04\text{ mM trypsin}$). The dialysis bags with 1 mL of DOX/np-4 solution were immersed in tubes containing 20 mL of buffer solution, with continuous shaking at $37\text{ }^\circ\text{C}$ ($n = 3$). At specific interval time points, 1 mL of the

external medium in the tube was collected as the sample and replenished with 1 mL of fresh medium. The DOX concentration was determined using a fluorescence spectrophotometer (Hitachi F-7000, Japan) with an excitation wavelength at 480 nm and emission wavelength at 550 nm.

2.7 Tumor cell uptake of DOX/np-4 and *in vitro* cytotoxicity assays

For the cellular uptake study, HT-29 cells were seeded into confocal dishes (35×12 mm, NEST Biotech Co, Ltd, China) at a density of 5×10^4 cells per dish for 24 h, and then incubated with DOX or Dox/np-4 (DOX-equivalent dose: $10 \mu\text{g mL}^{-1}$) for 1 and 4 h. After incubation, the cells were washed with PBS and stained with Hoechst 33342 for CLSM observation.

To evaluate the cytotoxicity of the nanoparticles, a Cell Counting Kit (CCK-8) assay was performed. The protocol was as follows: HT-29 or L929 cells were cultured in RPMI-1640 medium containing 10% fetal bovine serum (FBS) and 1% penicillin-streptomycin solution at 37°C under a humidified atmosphere of 95% air and 5% CO_2 . The cells were seeded at a density of 5×10^3 cells per well in 96-well plates for 24 h. Then, a suspension of particles in fresh medium was added to the cells with a series of concentrations for 24 h. After incubation, the culture medium from each well was removed, washed with PBS three times and 10% CCK8 was added to each well, followed by incubation for further 2 h. After that, the optical absorbance was then measured at 450 nm and the percentage of cell viability was calculated.

2.8 Animal experiments

For the *in vivo* study of the prepared np-4, female athymic nude BALB/c and BALB/c mice (4–7 weeks old, ~ 20 g) were obtained from Dashuo. All experiments with live animals were performed in compliance with the relevant laws and institutional guidelines of Sichuan University and were approved by the ethics committee of the Sichuan University. The HT-29 cells (5×10^6 cells per site) were implanted subcutaneously into the nude BALB/c mice to construct the HT-29 models. The 4T1 xenograft tumor model was generated by injecting 5×10^5 cells into the BALB/c mice. For the HT-29 tumor suppression study, the mice were administered different formulations at an equivalent dose of 2.5 mg doxorubicin per kg of mouse body weight when the tumor volume reached $50\text{--}100 \text{ mm}^3$. Catechins and np-4 were administered *via* intraperitoneal injection. Saline, DOX-HCl and Dox/np-4 were administered *via* intravenous injection. For the 4T1 tumor suppression study, the mice were intravenously injected with DOX-HCl and Dox/np-4 at an equivalent dose of 5.0 mg doxorubicin per kg of mouse body weight when the tumor volume reached $50\text{--}100 \text{ mm}^3$. The tumor growth was monitored by measuring the perpendicular diameter of the tumor using calipers. The tumor volume (mm^3) was calculated as $V = (L \times W^2)/2$, in which L and W indicate the length and width of the tumor.

***Ex vivo* imaging.** To investigate the distribution of DOX fluorescence at the organs and tumor sites, *ex vivo* imaging was performed. DOX and DOX/np-4 (equivalent of 5 mg kg^{-1} DOX)

were injected intravenously to the HT-29 tumor-bearing nude mice. After administration for 24 h, the animals were sacrificed and the tissues were isolated, and then imaged using a Maestro *In Vivo* Imaging System.

3. Results and discussion

3.1 Precise size tunability

The molecular assembly was actually a concentration-programmed approach for preparing size-controlled, functional catechin-keratin nanoparticles. The modulating effects of keratin-, catechin- or formaldehyde-dependent concentration on particle size were separately investigated with the concentrations of the other two components unchanged, and these modulating effects are schematically illustrated as three groups in Fig. 2a. In the keratin group, the nanoparticles of np-1, np-2 and np-3 were prepared at 5.0 mg mL^{-1} catechin and 0.1 mol L^{-1} formaldehyde with varying concentrations of keratin from 0.02 , 0.1 and 0.2 mg mL^{-1} , respectively. The corresponding hydrodynamic diameter by dynamic light scattering (DLS) measurements is 232 nm ($\text{PDI} = 0.012$) for np-1, 198 nm ($\text{PDI} = 0.089$) for np-2 and 158 nm ($\text{PDI} = 0.048$) for np-3. They dispersed as uniform spherical particles with narrow size distribution, which was further confirmed through SEM observations of the samples (Fig. 2b-d and Fig. S1-S3, ESI[†]). The TEM images together with the DLS data in Fig. 2e-g and e1-g1 show three kinds of nanoparticles of size 86 nm ($\text{PDI} = 0.168$) for np-4, 67 nm ($\text{PDI} = 0.121$) for np-5 and 31 nm ($\text{PDI} = 0.151$) for np-6, respectively, prepared from solutions of 5.0 mg mL^{-1} catechin and 0.1 mg mL^{-1} keratin with formaldehyde varying from 0.05 , 0.02 to 0.004 M (formaldehyde group). A similar trend that size follows a formaldehyde concentration-dependent fashion is also achieved in the catechin group. As shown in the TEM images and DLS data of Fig. 2h, i, h1 and i1, the size of the nanoparticles is 76 nm ($\text{PDI} = 0.155$) for np-7 and 43 nm ($\text{PDI} = 0.122$) for np-8, prepared from solutions of 0.1 mg mL^{-1} keratin and 0.1 M formaldehyde with either 2.5 mg mL^{-1} or 1.0 mg mL^{-1} catechin, respectively. The low magnification as-received SEM and TEM images are also given in Fig. S1-S8 (ESI[†]). When the concentration of catechin further reduced to 0.5 mg mL^{-1} , the size of the nanoparticles is only 30 nm (Fig. S9, ESI[†]). The SEM and TEM images of these nanoparticles show good dispersity, uniformity and sphericity, in agreement with the DLS results. A slightly larger size was shown in the DLS measurements than that from the SEM and TEM analysis due to the hydrated nanoparticles in water. The nanoparticle productivity was further calculated by using the Folin-Ciocalteu method in which catechin was used to obtain the standard curve (Fig. S10, ESI[†]), and the measured values are given in Table S1 (ESI[†]). The productivity values of these nanoparticles all exceed 60% in the keratin group. In contrast, with the decrement in the respective concentration, the productivity values of the nanoparticles in the catechin group and the formaldehyde-group gradually decreases.

3.2 Formation mechanism and molecular assignment

The mechanistic study of particle formation was performed on the formaldehyde-dependent system through observation and

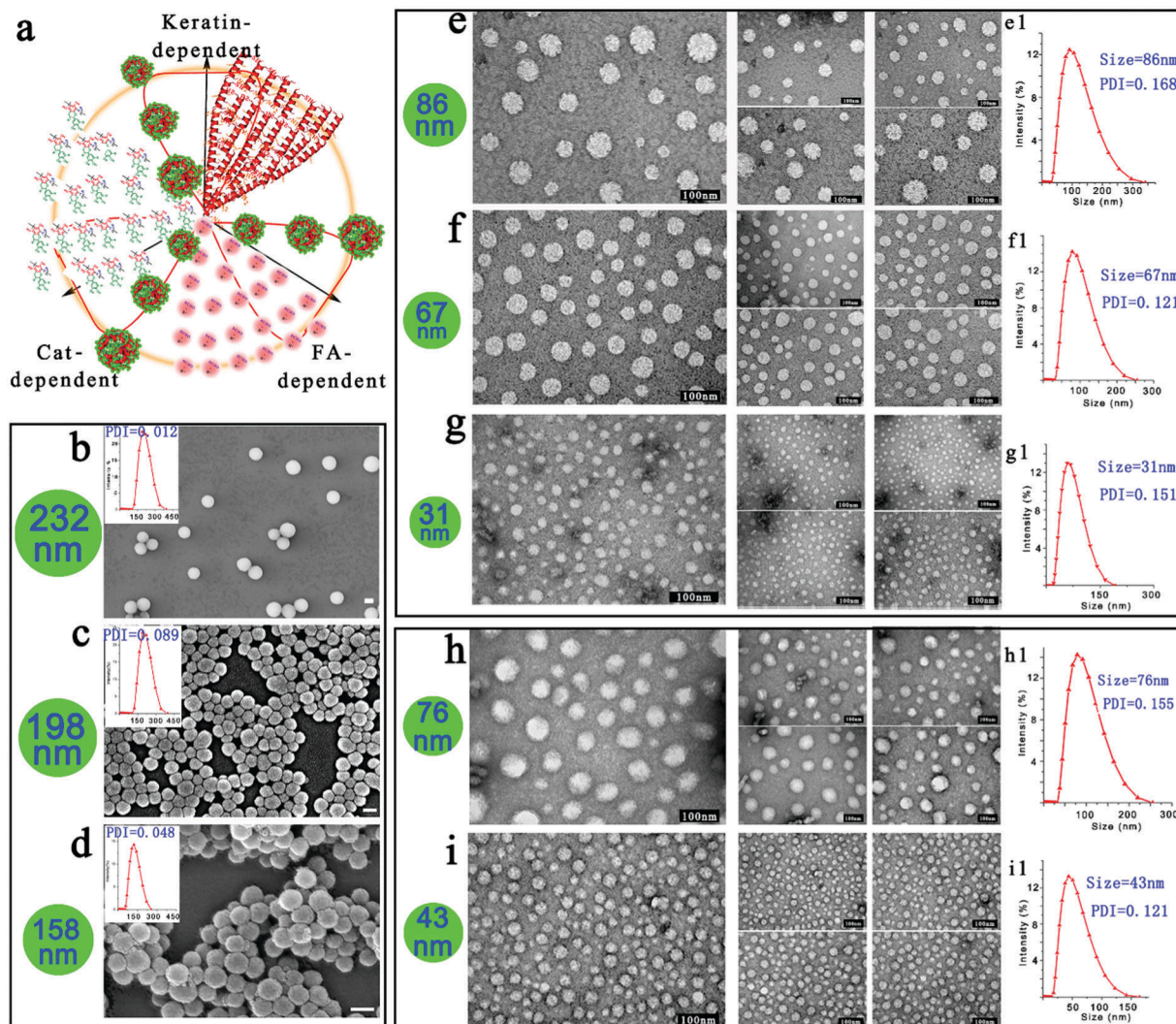


Fig. 2 (a) Schematic illustration of the modulating effects of keratin- or formaldehyde- or catechin-dependent concentrations on the nanoparticle size. SEM images of keratin-dependent nanoparticles with different sizes: (b) 232 nm (np-1), (c) 198 nm (np-2) and (d) 158 nm (np-3) (scale bar 200 nm). The inset represents DLS size distribution and PDI value. TEM images of formaldehyde-dependent nanoparticles with different sizes: (e) 86 nm (np-4), (f) 67 nm (np-5) and (g) 31 nm (np-6), and catechin-dependent nanoparticles: (h) 76 nm (np-7) and (i) 43 nm (np-8) (scale bar 100 nm). (e1–i1) DLS size distribution and PDI value corresponding to (e–i). Key parameters of the nanoparticles and low magnification images are given in Table S1 and Fig. S1–S8 (ESI†).

DLS measurements of the captured reactions at different intervals. Fig. 3a and b are the cartoon modes and respective photos of the reactions for np-2 captured at 1 h (colorless), 4 h (transparent blue), 8 h (light opalescent) and 12 h (opalescent suspension without precipitates). The appearance of a light blue color indicates the onset of nanoparticle formation. The continuous formation and growth of the nanoparticles at prolonged reaction intervals were further monitored by size measurements with DLS of reactions containing 5.0 mg mL⁻¹ catechin and 0.1 mg mL⁻¹ keratin with a varying concentration of formaldehyde from 0.1, 0.05, 0.02, 0.008 to 0.004 M (Fig. 3c). Again, these data confirm the conclusion from Fig. 2 that the size of the nanoparticles follows a formaldehyde-dependent concentration fashion. Meanwhile, the variation in the hydrodynamic diameters of the nanoparticles in opalescent suspensions collected at 12, 24,

36 and 60 h is narrow in all the formaldehyde-dependent cases, suggesting that the reaction within the period of 12 h is crucial for nanoparticle formation. The morphological evolution of the nanoparticles was also speculated. It is noteworthy that the coexistence of worm-like particles appears in the np-7 nanospheres (Fig. 2h and Fig. S11, ESI†). These worm-like particles have a relatively well-defined shape, ~10–20 nm in width, but are rather polydisperse in length, ranging from 10 to 100 nm. According to the highlights in Fig. S11 (ESI†), we tentatively propose the following evolution process for step-growth nanoparticle formation, the cartoon models and their TEM images of the relevant intermediates and final shapes are given from left to right in Fig. 3d. At first, formaldehyde initiates molecular interactions between keratins and catechins, yielding ultra-small nanoparticles of ~10 nm in size. Then, these ultra-small

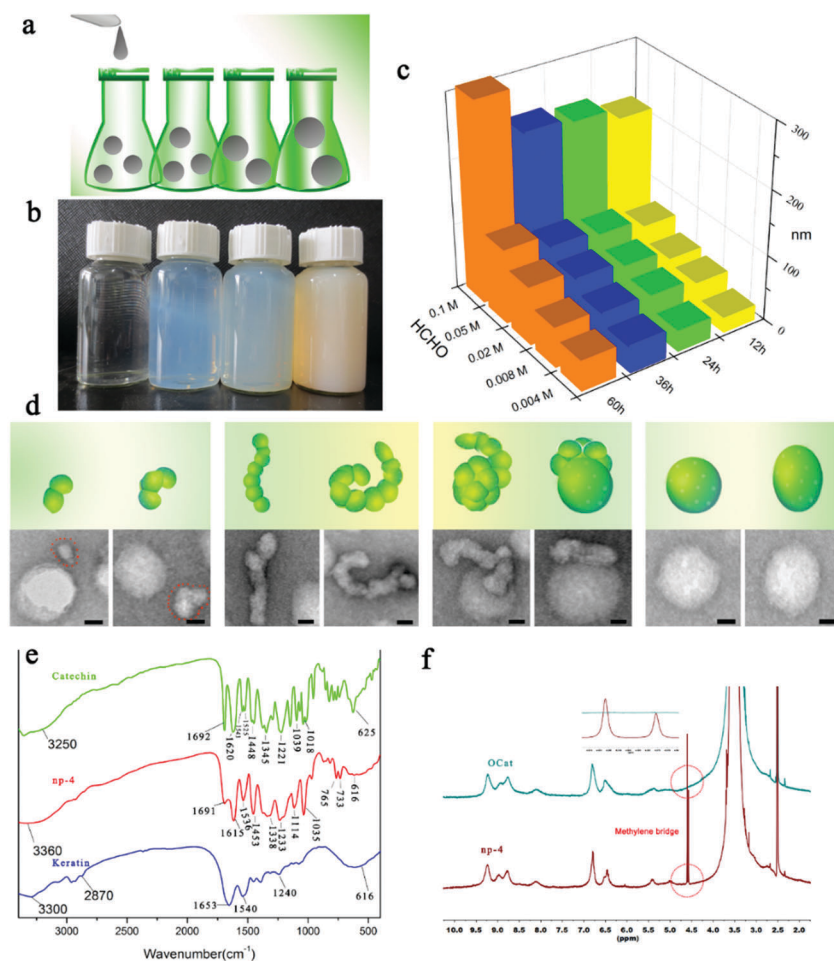


Fig. 3 (a) Cartoon modes and (b) photographs of the capturing reactions for np-2 at 1, 4, 8 and 12 h. (c) Size by DLS of intermediates from the reactions of 5.0 mg mL^{-1} catechin and 0.1 mg mL^{-1} keratin with different concentrations of formaldehyde captured at 12, 36, 48 and 60 h. (d) Cartoon models and their corresponding TEM images of intermediates and final shapes, illustrating the hypothesized mechanism of step-growth nanoparticles (scale bar 20 nm). (e) FT-IR spectra of keratin, catechin and np-4. (f) ^1H -NMR spectra of np-4 and oligomeric catechins (OCat), confirming the occurrence of catechin oligomerization and methylene bridged amino acids.

nano-particles act as seeds to grow continuously due to the addition reaction of protein and polyphenol, into different intermediates, which finally evolve into spheric nanoparticles. The transformation of intermediates into spheres is governed by the minimum surface energy principle. The presence of intermediates constituted by discernible two or three ultra-small nanoparticles suggests that the growth of the nano-particles actually proceeds by aggregation of ultra-small nanoparticles as primary building blocks. In fact, the observation of worm-like nanoparticles validates the occurrence of consecutively linear aggregation of the building blocks. Moreover, the size of the nanoparticles is dependent upon the concentrations of the reactive constituents. The reactions at a higher concentration of keratin proteins correspond to more nucleation sites, thus giving rise to smaller nanospheres. When a higher concentration of catechins is further introduced, the reactions actually occur at a diluted concentration of keratins. In this case, fewer nucleation sites are formed, and thus the final products are larger nanospheres produced due to consecutive aggregation of the reactive constituents. The reactions proceed at a lower

concentration of formaldehyde, corresponding to less reaction activity, and thus leading to the smaller nanospheres. In contrast, the feedstock solutions in the absence of any one of three constituents keep a clear state (see Table S1, ESI[†]).

The SDS-PAGE in Fig. S12 (ESI[†]) shows that the keratins extracted from human hair fibers mainly consist of keratins and matrix proteins, with molecular weights of 40–60 kDa and 15–30 kDa.²⁹ According to the FT-IR spectra in Fig. 3e, the adsorptions at 1653 , 1540 and 1240 cm^{-1} are observed in keratins, attributable to amide I, II and III, respectively.³⁵ These characteristic adsorptions of keratins are overlapped with those of catechins, thus hardly discernible in np-4. But, the presence of a strong adsorption centered at 616 cm^{-1} , ascribed to the C-S stretching vibrations, validates the incorporation of keratins in the prepared nanoparticles.³⁰ Multiple sharp adsorptions are present in the spectrum of the catechins. In contrast, molecular interactions for the preparation of np-4 lead to the shifting, broadening and disappearance of some characteristic adsorptions of catechins, indicative of the oligomerization of the catechins. In np-4, the stretching vibrations of the aromatic

ring C-C/C=C appears at 1615, 1536 and 1453 cm^{-1} , the broadening C-H bending vibrations are centered at 1338 cm^{-1} and the stretching vibrations of aromatic ether are located at 1233, 1114 and 1035 cm^{-1} .³⁶ In addition, the deformation vibrations of the C-H bonds in the benzene ring at 1148, 1067 and 787 cm^{-1} completely disappear. The enhanced adsorption at 1453 cm^{-1} along with the presence of absorptions at 765 and 733 cm^{-1} shows the formation of methylene bridges.³⁷ Fig. 3 shows the ^1H NMR spectra of the np-4 nanoparticles with oligomeric catechins (OCat) as a reference. The broad peaks in oligomeric catechins suggest that each polymer unit has a slightly different chemical environment. The spectral similarity between the oligomeric catechins and np-4 confirms the occurrence of oligomerization of the catechins in the preparation of the nanoparticles. Furthermore, in the spectrum of np-4 the peaks appear with a maxima at 9.2, 8.9, 8.7 and 8.1 ppm, corresponding to the -OH groups of the benzene ring. The peaks at 6.8 and 6.5 ppm are assigned to hydrogen at 2' and 6' on the B-ring and D-ring, respectively. The peaks at 5.4 and 5.0 ppm are assigned to the hydrogen at positions 3 and 2 on the C ring.^{38,39}

In fact, the present ^1H NMR spectra are in agreement with the previously reported oligomeric EGCG.^{8,40} Furthermore, two new peaks at 4.5 and 4.6 ppm in the ^1H NMR spectrum of np-4 are attributable to the methylene bridged bonds between the amino acids Lys and Cys.⁴¹ All the UV-vis spectra (Fig. S13, ESI[†]) of the np-1 to np-7 nanoparticles give a maximum absorbance at ~ 280 nm, confirming the presence of polyphenolic compounds in the nanospheres. Fig. S14 (ESI[†]) shows the ζ -potential values of np-2, np-4, np-5, np-7 and np-8, typical nanoparticles of keratin-, catechin- and formaldehyde-dependent cases, in a series of buffer solutions with different pH values. The measured values are in the range of -16 to -30 mV, and steadily increase with buffer solutions with elevating pH values from 3.0 to 8.0, indicative of the existence of catechins. As formaldehyde was used to trigger the covalent interactions of catechins and keratins for the molecular assembly of nanoparticles, the potential residue of formaldehyde in the nanoparticles was analyzed using HPLC. According to Fig. S15 (ESI[†]), almost no residual formaldehyde was detected even in 4 g L^{-1} np-4 nanoparticles, suggestive of no health risk associated with the consumption of those nanoparticles.

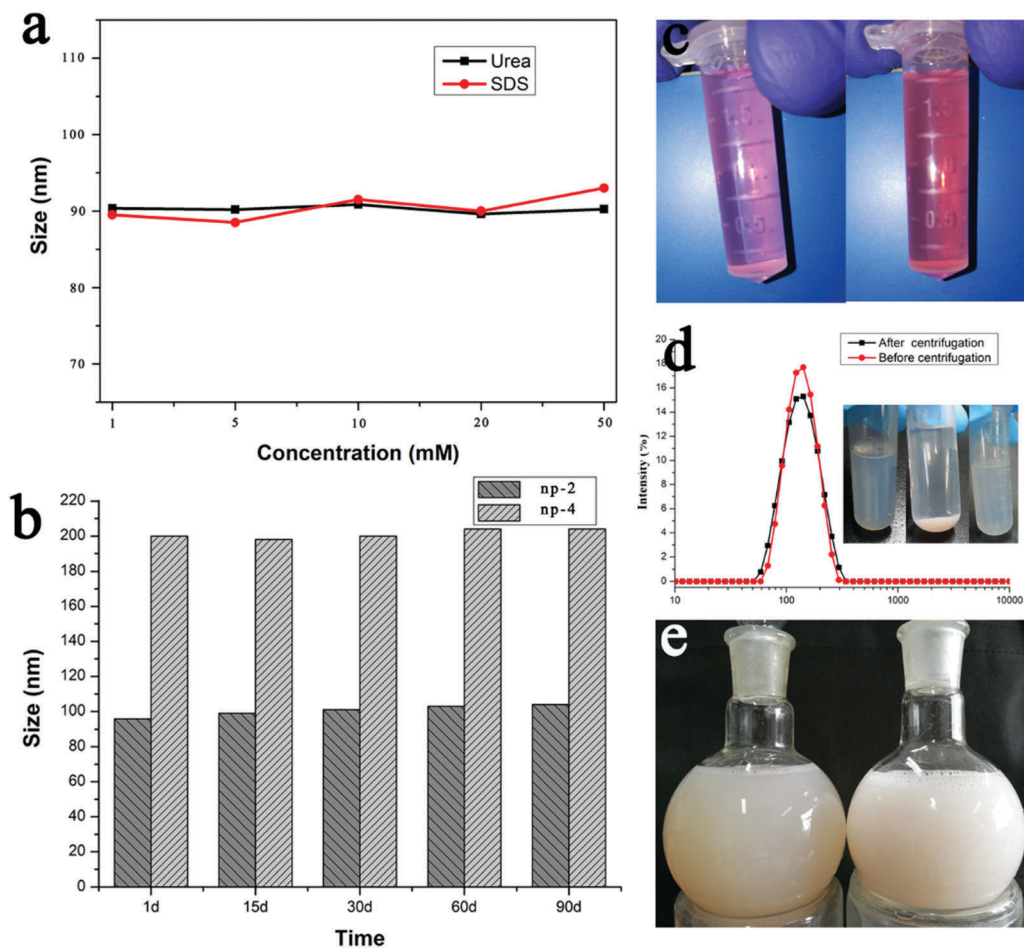


Fig. 4 (a) The size vs. concentration curves of np-4 at different concentrations of urea or SDS for 2 h, revealing predominant covalent interactions for the molecular assembly of nanoparticles. (b) The long-term stability (\sim up to 90 d) of np-2 and np-4 well-dispersed in water at 4 $^{\circ}\text{C}$. Photographs of (c) np-4 (left) and np-4 loaded with anticancer drug-doxorubicin (right) in 1640 medium with 10% FBS for 24 h, (d) DLS results of nanoparticles before collection and after re-dispersion, the inset shows the easy collection of reaction products by using salting-out method and subsequent easy dispersion of nanoparticles in solution, and (e) photographs exhibiting the large-scale preparation of nanoparticles.

3.3 Colloidal behaviors

The behaviors of nanoparticles in different solutions were further investigated by applying DLS to measure their hydrodynamic diameters, and the results are given representatively with np-4. Fig. 4a shows the size vs. concentration curves of the np-4 nanoparticles incubated in solutions containing different concentrations of sodium dodecyl sulphate (SDS) or urea. The size of np-4 almost remains unchanged after 2 h of incubation either in SDS or in urea with concentrations varying from 1.0, 5.0, 10.0, 20.0 to 50.0 mM. Fig. S16 (ESI[†]) shows the comparative photos of pure keratins and np-4 in absolute ethyl alcohol. The addition of keratin was found to cause immediate precipitation whereas the np-4 nanoparticles were well dispersed in ethyl alcohol. Hydrophobic competition is strong for SDS, and urea is capable of participating in the formation of strong hydrogen bonds. Meanwhile, ethanol as a semipolar solvent is found to interfere with polyphenol-protein complexation.⁴² The DLS measurements did not detect any obvious size variation of the np-4 nanoparticles in either SDS or urea solutions and in absolute ethyl alcohol, confirming that the predominant mode of the underlying interactions for the molecular assembly of nanoparticles is covalent interactions as illustrated in Fig. 1, rather than other interactions such as hydrogen bonding or hydrophobic interactions. Fig. 4b shows that the nanoparticles, either np-2 of 201 nm or np-4 of 90 nm, have excellent long-term colloidal stability after dispersion in water for up to 90 d at 4 °C. Fig. 4c further shows that both np-4 and anticancer drug loaded np-4 (DOX/np-4) are still colloidally stable when incubated in the 1640 culture medium with 10% FBS for 24 h. Fig. 4d verifies that a good polydisperse index was achieved by re-dispersion of

nanoparticles collected using a salting-out method in water. The inset photos of Fig. 4d demonstrate that the collection of synthetic nanoparticles from reactions is quite simple and convenient. Fig. S17 (ESI[†]) shows that the polydisperse index remains nearly constant. Thus, a large-scale production of nanoparticles can be easily realized (Fig. 4e), laying solid foundations for various biomedical purposes.

3.4 Dual stimuli-responsive properties

The combination of keratins with catechins yields biocompatible, biologically responsive nanoparticles with therapeutic effects. Fig. 5a shows the bar diagram of the hydrodynamic diameters of np-4 in the presence of a varying glutathione (GSH) concentrations, measured by DLS under physiological conditions at different intervals of 30 min, 2 h, 6 h and 24 h. The change in the hydrodynamic diameter is related to the swelling of the nanoparticles. In 10 μM GSH, almost no variation in size was recorded for all the incubation intervals, and the size of the np-4 samples was maintained at about 90 nm. With elevating GSH concentrations of up to 2 mM, the increments in size is still negligible for incubations of np-4 up to 6 h. Obvious swelling appears in the samples incubated for 24 h, where the measured diameter is 380 nm, 3 times larger than the original size. When the nanoparticles were incubated in 5 mM GSH, no swelling occurred after 30 min, but the size increased to 200 nm after 2 h and increased abruptly up to 580 nm after 6 h. An even longer incubation led to the production of floccules, resulting from the rupture of swollen spheres, and thus no data were given for the interval of 24 h. In contrast, the recorded size of the nanoparticles is 200 nm for 30 min and 350 nm for 2 h of

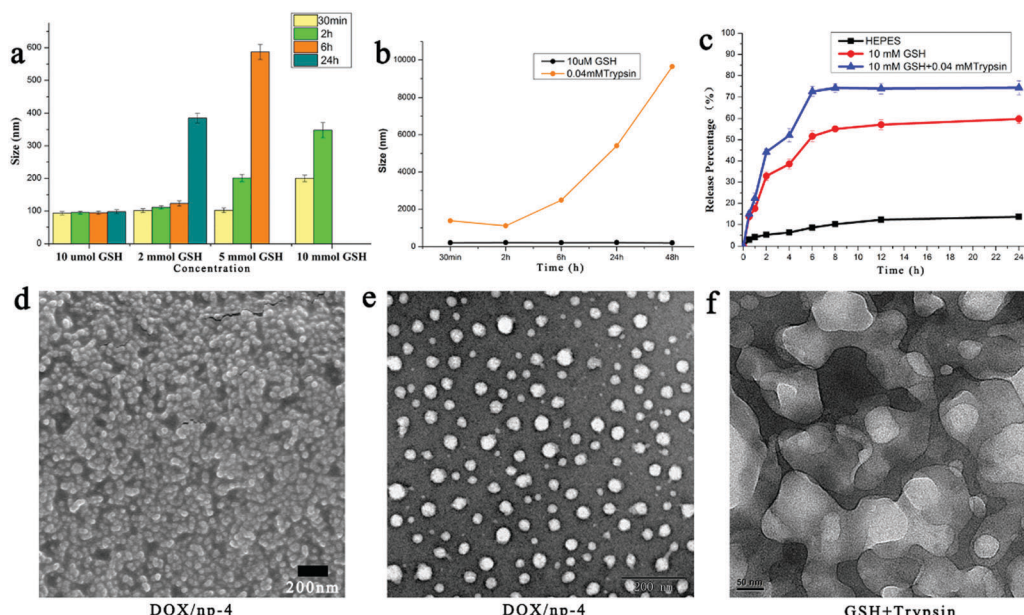


Fig. 5 Size of the np-4 nanoparticles by DLS measurements incubated (a) at GSH concentrations ranging from extracellular to intracellular environment and (b) at 0.04 mM trypsin under pathological conditions (cancer or inflammation) in comparison with 10 μM GSH (black line) for different incubation intervals. (c) The release profiles of DOX released from DOX/np-4 nanoparticles in pH 7.4 HEPES, 10 mM GSH and 10 mM GSH + 0.04 mM trypsin buffer solutions as a function of time. Comparative (d) SEM and (e) TEM images of the DOX/np-4 nanoparticles and (f) TEM image of the corresponding nanoparticles after incubated with 10 mM GSH + 0.04 mM trypsin (GSH + trypsin).

incubation in 10 mM GSH. Fig. S18 (ESI†) supplements these results visually with photos to reveal the different GSH-responsive phenomena of np-4 after incubation for 4 h. This GSH-responsive swelling behavior of nanoparticles is primarily due to the cleavage of disulfide bonds in keratin proteins by GSH reducing activities. On the other hand, keratin is rich in lysine and arginine, which means that it can be cleaved by trypsin *in vivo*.⁴³ As shown in Fig. 5b, the diameter of the np-4 nanoparticles quickly increased in the presence of 0.04 mM trypsin, but remains almost unchanged in 10 μM GSH. The concentration of GSH varies depending upon a specific location, *e.g.*, about 10 mM in the cytosol of tumor/cancer cells, but ranging from 1 to 10 μM in extracellular plasma and normal tissues.⁴⁴ The DOX release profiles of DOX/np-4 were evaluated in different biomimetic buffer solutions at 37 °C. As shown in Fig. 5c, a negligible amount of DOX was detected in HEPES buffer. In contrast, the addition of GSH and trypsin caused rapid release of DOX from the np-4. After incubation for 6 h in 10 mM GSH and 10 mM GSH + 0.04 mM trypsin, almost 53% and 74% of DOX was released from np-4, respectively. The release behavior of np-4 is similar to other nanocarriers that respond to enzymes.^{45,46} The SEM and TEM images (Fig. 5d and e) of DOX/np-4 reveals that the loading of DOX does not cause an obvious change in either the size or morphology of the nanoparticles. In contrast, after treatment with GSH and trypsin the nanoparticles were completely disassembled (Fig. 5f). Accordingly, the present covalently-assembled nanospheres are intelligent carriers, stable under normal physiological environments but swelling that can be broken at tumor sites, ideal for targeted delivery of anticancer drugs.

3.5 Cellular uptake and *in vitro* anti-tumor activity

To assess the intracellular distribution of DOX/np-4, the HT-29 cells were incubated with DOX/np-4 and free DOX at an equivalent DOX concentration of 10 μg mL⁻¹ for 1 and 4 h, respectively. The confocal laser scanning microscopy (CLSM) images give the DOX distribution in the cytosol and nucleus of the HT-29 cells treated with DOX/np-4 and DOX. As shown in Fig. 6a, after incubation for 1 h and 4 h the red fluorescence of DOX was observed strongly in the cytoplasm and nucleus of the DOX groups. In the DOX/np-4 groups, the DOX fluorescence signals mainly existed in the cytoplasm after the first one hour but were not found in the cell nucleus. In contrast, after incubation for 4 h, the fluorescence signal in the nucleus already became strong. The results demonstrate that these nanoparticles could be efficiently taken up by cancer cells and subsequently that the nanoparticles degraded to release the guest molecules under an intracellular environment. The release behavior of np-4 as drug carriers is triggered by GSH- and enzyme-responsive properties. The cytotoxicity of nanocarriers was investigated in normal mouse fibroblast cells (L929 cells). As shown in Fig. 6b, when the dose of nanoparticles was below 40 μg mL⁻¹, the nanoparticles are biocompatible.

As tea polyphenols have strong anticancer capabilities, the comparative inhibitory effect of pure catechins and np-4 nanoparticles on the proliferation of colon cancer lines HT-29 was

quantitatively assessed using a CCK 8 assay. Fig. 6c shows the plot of the cell viabilities of HT-29 cells incubated separately with pure catechins and with np-4 nanoparticles at different dosages for 24 h. The np-4 nanoparticles are shown to have comparable inhibition effects to pure catechins in a dosage-dependent manner, confirming that the present nanoparticles also have therapeutic effects. Next, we present the use of np-4 nanoparticles as functional carriers to deliver doxorubicin hydrochloride (DOX) for cancer therapies. DOX is a DNA targeting toxin, the effective accumulation of DOX in the nucleus as shown in Fig. 6a is thus expected to have high cytotoxicity towards cancer cells. In fact, the comparative cell viabilities of the HT-29 cells treated with free DOX and DOX/np-4 at different dosages for 24 h validates the fact that DOX/np-4 exhibits a higher inhibition rate than free DOX (Fig. 6d). The IC₅₀ value (the concentration causing 50% growth inhibition) given in the inset is 0.66 μg mL⁻¹ for DOX/np-4 and 0.86 μg mL⁻¹ for free DOX.

3.6 *In vivo* antitumor activity

In order to prove that the present colloidally stable but dual stimuli-responsive nanospheres are useful for anticancer drug delivery, we performed *ex vivo* fluorescence imaging of major organs and tumor tissues isolated from the HT-29 tumor-bearing mice intravenously injected with DOX/np-4 and free DOX. After administration for 24 h, the heart, liver, spleen, lungs, kidneys and tumors were dissected from the treated mice to determine the distribution of the drug by *ex vivo* fluorescence imaging. As shown in the images in Fig. 7a and b, apart from the heart, DOX/np-4 exhibited stronger fluorescence signals than DOX in all tissues. The semi-quantitative data based on the *ex vivo* imaging of resected organs and tumors further showed that the total fluorescence intensity of DOX was stronger in the DOX/np-4 group than in the DOX group (Fig. 7c). This result demonstrates that DOX/np-4 could resist the rapid clearance and thus extend the half-life of the loaded DOX. Fig. 7d quantitatively exhibits the comparative fluorescence intensity of each organ. Compared to the DOX group, the signal intensity of DOX from the DOX/np-4 group was obviously stronger in all of the tissues. This phenomenon is most significant especially in the tumor sites where a large amount of the drug was accumulated in the DOX/np-4 group. In contrast, after a long period of metabolism by the organism, the DOX signal in the tumor sites from the DOX group became very weak. These results imply that the catechin-based nanocarriers are successful in effectively targeting tumor sites.

In vivo anticancer activities of DOX/np-4 and np-4 were further investigated in comparison with pure catechin and free drugs by using different tumor-xenografted mice models. The HT-29 xenografted athymic nude mice were treated either with saline, catechins (50 mg kg⁻¹) and np-4 (containing equivalent dose of catechins) *via* i.p. administration or with DOX (2.5 mg kg⁻¹) and DOX/np-4 (equivalent DOX 2.5 mg kg⁻¹) *via* i.v. injection. During the 18 d evaluation period, the tumor treated with saline continues to grow. In contrast, i.p. administration of pure catechins and np-4 gives an 18.8% and 63.3% tumor growth inhibition rate, respectively. In addition, the tumor

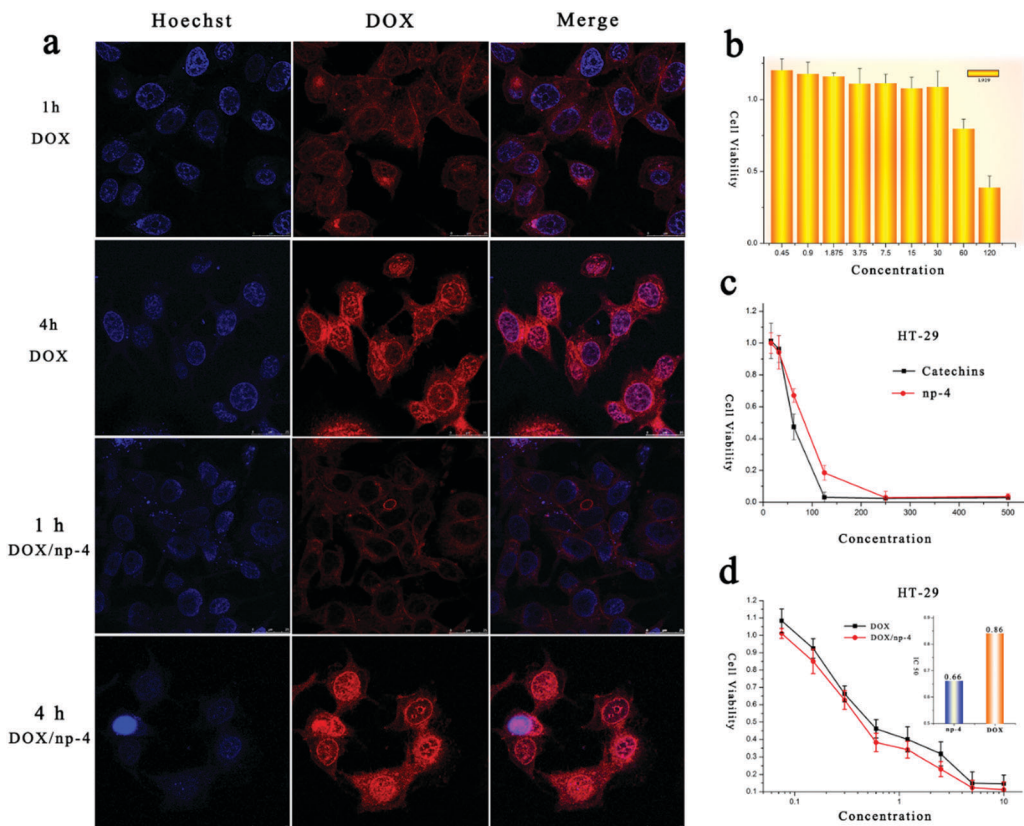


Fig. 6 (a) CLSM images showing the DOX distribution in cytosol and nucleus of the HT-29 cells treated with free DOX and DOX/np-4 for 1 and 4 h. (b) Viabilities of the L929 cells incubated with a varying concentration of np-4 after culturing of 24 h. (c) Viabilities of the HT-29 cells treated with pure tea polyphenols (catechins) or np-4 for 24 h. (d) Viabilities of the HT-29 cells treated with free DOX and DOX/np-4 at different dosages for 24 h. The inset is IC₅₀ value of DOX and DOX/np-4 to HT-29 cells.

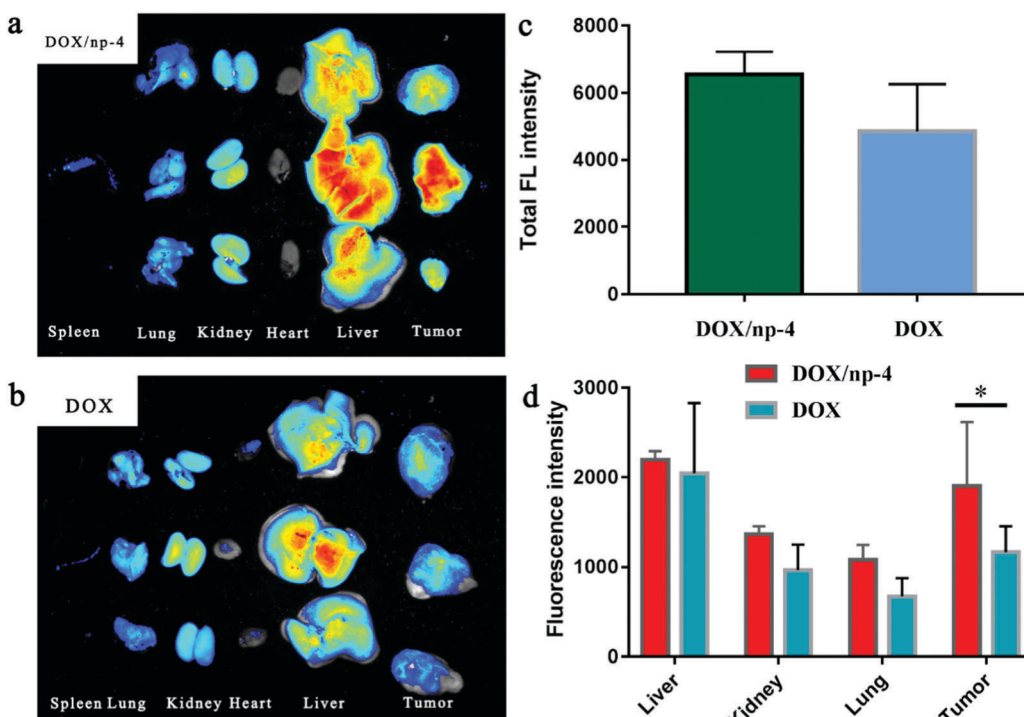


Fig. 7 Ex vivo DOX biodistribution in isolated tissues from the HT-29 tumor-bearing nude mice after intravenous injection of (a) DOX/np-4 and (b) DOX for 24 h. Semi-quantitative data of fluorescence intensity: (c) total intensity and (d) in different tissues ($n = 3$).

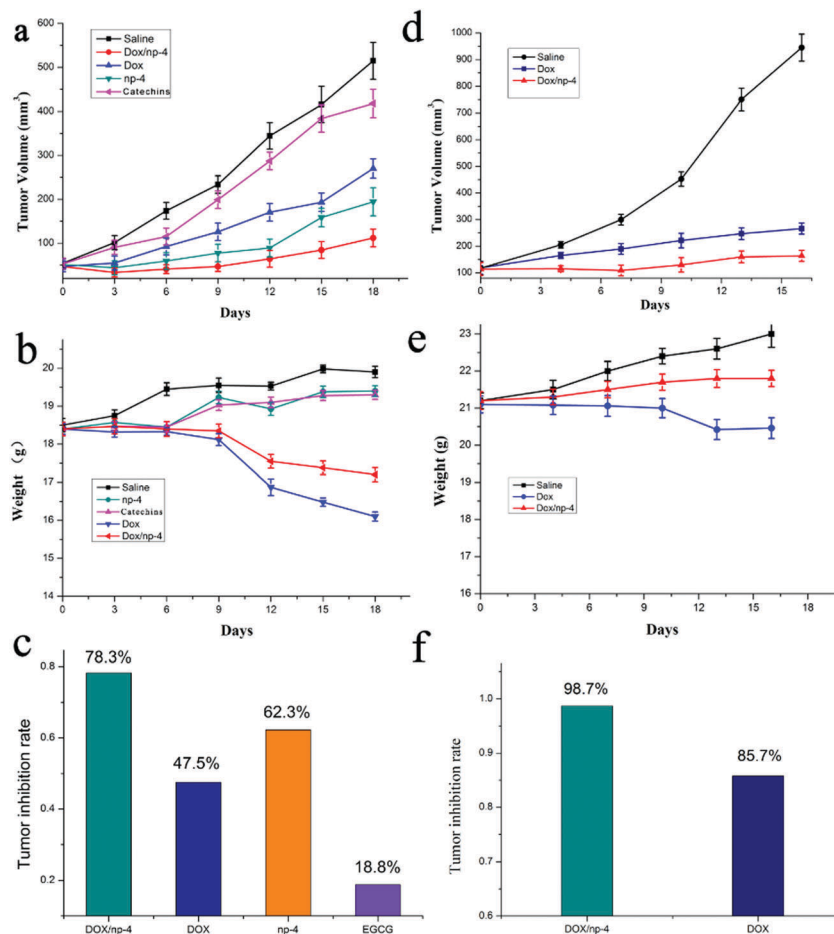


Fig. 8 (a) Tumor volume change of the HT-29 colon tumor model. Bab/c female athymic nude mice with subcutaneous tumors from the colon cancer cells were treated either with saline, catechins (50 mg kg^{-1}) and np-4 (equivalent catechin 50 mg kg^{-1}) via i.p. administration or with free DOX (2.5 mg kg^{-1}) and DOX/np-4 (equivalent DOX 2.5 mg kg^{-1}) via i.v. administration. (b) Body weight change of the Bab/c female athymic nude mice. (c) The tumor inhibition rate of the HT-29 tumor model. (d) Tumor volume changes of a mouse 4T1 breast tumor model. Bab/c mice with subcutaneous tumors from 4T1 cancer cells were treated with saline, DOX (5 mg kg^{-1}) and DOX/np-4 (equivalent DOX 5 mg kg^{-1}) via i.v. administration. (e) Body weight change of Bab/c mice. (f) The tumor inhibition rate of the 4T1 tumor model.

growth inhibition rate with i.v. injection of free DOX was 47.5%, but this value with i.v. injection of DOX/np-4 was up to 78.3%, exhibiting the best anticancer effect. It is noteworthy that i.p. administration of pure np-4 shows a significantly higher anticancer effect than i.p. administration of equivalent pure catechins, and also higher anticancer effects than i.v. injection of free DOX (Fig. 8a and c). This result demonstrates that the molecular assembly of catechins and keratins into nanoparticles has a greatly pronounced efficacy on improving bioavailability of tea polyphenols.

Body weight loss is an indicator of systemic toxicity. As shown in Fig. 8b, the mice treated with free DOX have severe weight loss, confirming the serious systemic toxicity of the anticancer drug. A fair amount of body weight gain was observed in the mice treated with saline, pure catechins and np-4 (that is drug free), indicative of the biosafety of catechins and the present nanoparticles. In the case of the 4T1 xenografted Bab/c mice model (Fig. 8d and e), injected free DOX efficiently retards tumor growth. The corresponding tumor growth inhibition is 85.8%

relative to that of the saline control, but this inhibition is accompanied with a loss in body weight. In contrast, a tumor growth inhibition of 98.7% along with a slight increase in body weight is achieved in the 4T1 tumor-bearing Bab/c mice treated with DOX/np-4 (Fig. 8f). In the 4T1 model group, the tumors were isolated at the end of the treatment, photographed (Fig. S19, ESI†) and weighed (Fig. S20, ESI†). The tumor sizes and weights from the mice group administrated with DOX/np-4 were obviously smaller and lighter than those groups treated with free DOX and saline.

The antitumor activity of various formulations was further evaluated through histological observations of tumor tissues from HT-29 xenografted female nude mice (H&E, Ki-67 and CD 31 staining). As shown in Fig. 9, in the H&E stained column only few apoptotic or necrotic tumor cells were observed in the control group, but the necrotic area was increased in the catechin and np-4 groups. In the DOX group the inhibition became obviously high and a large area of tumor necrosis was found in the DOX/np-4 groups. Ki-67 protein is regarded as the most promising

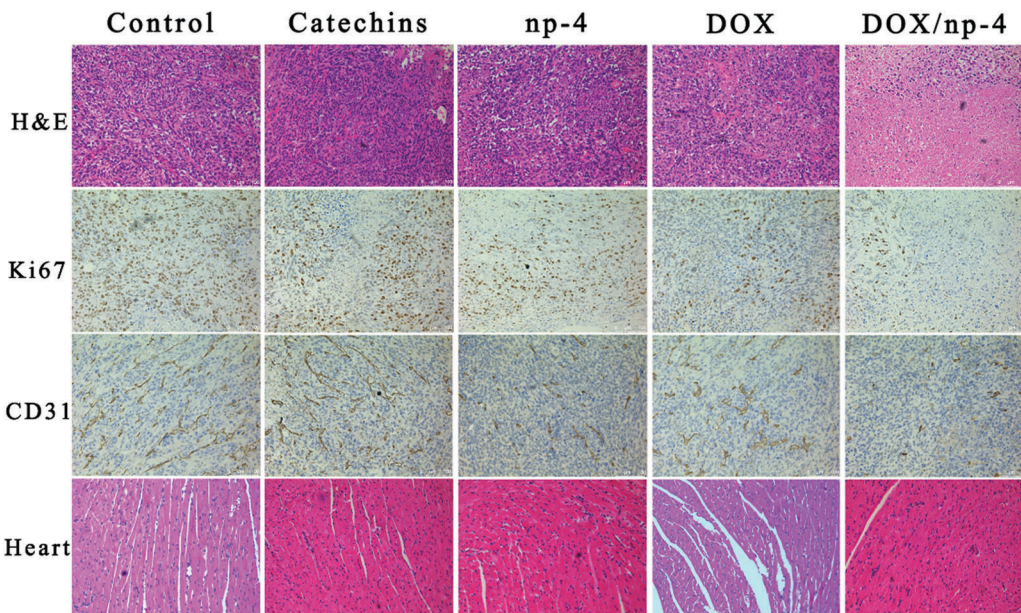


Fig. 9 Histological analyses of tumor tissues with H&E, Ki67 and CD31 stained tumor slices and heart tissues with H&E stained heart slices from the HT-29 xenografted female nude mice after treatment with various formulations.

biomarker for cell proliferation which is expressed in the proliferating cells during all active phases of the cell cycle. CD31 is a transmembrane glycoprotein and a platelet endothelial cell adhesion molecule, which recognizes preexisting and newly formed vasculature regardless of size in normal and tumor tissues with the same intensity.¹⁸ Compared with the saline control, all of the treatments groups decreased in the expression of Ki-67 and CD 31, and the catechins group decreased the least. The DOX and np-4 groups showed a moderate intensity reduction, and DOX/np-4 showed a significant decrease. In addition, administration of DOX can lead to severe side effects, and we therefore assessed the potential toxicity of DOX to heart tissues of the HT-29 xenografted female nude mice after different treatments. In the free DOX group the nude mice showed mild cardiac toxicity. In contrast, no appreciable histomorphological changes of the heart were observed after continuous administration of catechins, np-4 and DOX/np-4, indicating that np-4 as a nanocarrier could reduce the systemic toxicity of DOX.

4. Conclusions

In summary, we have demonstrated a simple one-pot method for large-scale, rapid and precise preparation of biocompatible, multifunctional and size-tunable nanoparticles using naturally reproducible green tea polyphenols and keratin proteins. These nanoparticles are spherical particles with a wide range of sizes (hydrodynamic diameter by DLS) from 30 nm to 230 nm, tuned simply by different concentration combinations of catechin, keratin and formaldehyde. Owing to the covalent interactions of catechins and keratins for molecular assembly, these nanospheres are long-term colloidally stable in water, but are disassemble sensitive to GSH and enzyme. The nanoparticles (np-4) are representatively selected as carriers for loading the

cancer drug DOX, and their anticancer activities both *in vitro* and *in vivo* were investigated, confirming that DOX-loaded nanoparticles give a combination of enhanced effects in cancer treatments with much less systemic toxicity than free DOX. Most importantly, the present study permits a large-scale preparation of nanoparticles with a wide range of tunable sizes, thus their functional effects, fates and other biological performances could be systematically assessed in the future. This study actually offers an innovative strategy to make good use of naturally reproducible green tea polyphenols *via* molecular assembly with keratin proteins into functional nanoparticles, which are promising for a variety of applications including for therapeutic and preventive purposes.

Conflicts of interest

The authors declare no competing financial interest.

Acknowledgements

This work was supported by the National Natural Science Foundation of China (No. 51373106), the National Basic Research Program of China (No. 2012CB933600), and the National Key Research and Development Program of China (No. 2016YFC1102700).

References

- 1 S. Nie, Y. Xing, G. J. Kim and J. W. Simons, Nanotechnology applications in cancer, *Annu. Rev. Biomed. Eng.*, 2007, **9**, 257–288.
- 2 H. Cabral, Y. Matsumoto, K. Mizuno, Q. Chen, M. Murakami, M. Kimura, Y. Terada, M. R. Kano, K. Miyazono, M. Uesaka,

- N. Nishiyama and K. Kataoka, Accumulation of sub-100 nm polymeric micelles in poorly permeable tumours depends on size, *Nat. Nanotechnol.*, 2011, **6**(12), 815–823.
- 3 M. Ferrari, Cancer nanotechnology: opportunities and challenges, *Nat. Rev.*, 2005, **5**(3), 161–171.
- 4 V. P. Torchilin, Multifunctional, stimuli-sensitive nanoparticulate systems for drug delivery, *Nat. Rev. Drug Discovery*, 2014, **13**(11), 813–827.
- 5 E. Fleige, M. A. Quadir and R. Haag, Stimuli-responsive polymeric nanocarriers for the controlled transport of active compounds: concepts and applications, *Nat. Rev. Drug Discovery*, 2012, **64**(9), 866–884.
- 6 S. Mura, J. Nicolas and P. Couvreur, Stimuli-responsive nanocarriers for drug delivery, *Nat. Mater.*, 2013, **12**(11), 991–1003.
- 7 T. M. Allen and P. R. Cullis, Drug Delivery Systems: Entering the Mainstream, *Science*, 2004, **303**, 1818–1822.
- 8 J. E. Chung, S. Tan, S. J. Gao, N. Yongvongsoontorn, S. H. Kim, J. H. Lee, H. S. Choi, H. Yano, L. Zhuo, M. Kurisawa and J. Y. Ying, Self-assembled micellar nanocomplexes comprising green tea catechin derivatives and protein drugs for cancer therapy, *Nat. Nanotechnol.*, 2014, **9**(11), 907–912.
- 9 E. A. Sykes, J. Chen, G. Zheng and W. C. W. Chan, Investigating the Impact of Nanoparticle Size on Active and Passive Tumor Targeting Efficiency, *ACS Nano*, 2014, **8**(6), 5696–5796.
- 10 W. Jiang, B. Y. Kim, J. T. Rutka and W. C. Chan, Nanoparticle-mediated cellular response is size-dependent, *Nat. Nanotechnol.*, 2008, **3**(3), 145–150.
- 11 A. Albanese, P. S. Tang and W. C. Chan, The effect of nanoparticle size, shape, and surface chemistry on biological systems, *Annu. Rev. Biomed. Eng.*, 2012, **14**, 1–16.
- 12 J. W. Hickey, J. L. Santos, J. M. Williford and H. Q. Mao, Control of polymeric nanoparticle size to improve therapeutic delivery, *J. Controlled Release*, 2015, **219**, 536–547.
- 13 S. Oliver, O. Vittorio, G. Cirillo and C. Boyer, Enhancing the therapeutic effects of polyphenols with macromolecules, *Polym. Chem.*, 2016, **7**(8), 1529–1544.
- 14 S. Quideau, D. Deffieux, C. Douat-Casassus and L. Pouysegur, Plant polyphenols: chemical properties, biological activities, and synthesis, *Angew. Chem., Int. Ed.*, 2011, **50**(3), 586–621.
- 15 C. S. Yang, X. Wang, G. Lu and S. C. Picinich, Cancer prevention by tea: animal studies, molecular mechanisms and human relevance, *Nat. Rev. Cancer*, 2009, **9**(6), 429–439.
- 16 S. Wang, R. Su, S. Nie, M. Sun, J. Zhang, D. Wu and N. Moustaid-Moussa, Application of nanotechnology in improving bioavailability and bioactivity of diet-derived phytochemicals, *J. Nutr. Biochem.*, 2014, **25**(4), 363–376.
- 17 J. Ding, J. Yao, J. Xue, R. Li, B. Bao, L. Jiang, J. J. Zhu and Z. He, Tumor-Homing Cell-Penetrating Peptide Linked to Colloidal Mesoporous Silica Encapsulated (−)-Epigallocatechin-3-gallate as Drug Delivery System for Breast Cancer Therapy in Vivo, *ACS Appl. Mater. Interfaces*, 2015, **7**(32), 18145–18155.
- 18 N. Khan, D. J. Bharali, V. M. Adhami, I. A. Siddiqui, H. Cui, S. M. Shabana, S. A. Mousa and H. Mukhtar, Oral administration of naturally occurring chitosan-based nanoformulated green tea polyphenol EGCG effectively inhibits prostate cancer cell growth in a xenograft model, *Carcinogenesis*, 2014, **35**(2), 415–423.
- 19 T. Cheng, J. Liu, J. Ren, F. Huang, H. Ou, Y. Ding, Y. Zhang, R. Ma, Y. An, J. Liu and L. Shi, Green Tea Catechin-Based Complex Micelles Combined with Doxorubicin to Overcome Cardiotoxicity and Multidrug Resistance, *Theranostics*, 2016, **6**(9), 1277–1292.
- 20 Y. H. Lin, Z. R. Chen, C. H. Lai, C. H. Hsieh and C. L. Feng, Active Targeted Nanoparticles for Oral Administration of Gastric Cancer Therapy, *Biomacromolecules*, 2015, **16**(9), 3021–3032.
- 21 Y. Huang, M. Sumida, M. Kumazoe, K. Sugihara, Y. Suemasu, S. Yamada, S. Yamashita, J. Miyakawa, T. Takahashi, H. Tanaka, Y. Fujimura and H. Tachibana, Oligomer formation of a tea polyphenol, EGCG, on its sensing molecule 67 kDa laminin receptor, *Chem. Commun.*, 2017, **53**(12), 1941–1944.
- 22 S. Cornwall, G. Cull, D. Joske and R. Ghassemifar, Green tea polyphenol “epigallocatechin-3-gallate”, differentially induces apoptosis in CLL B-and T-Cells but not in healthy B-and T-Cells in a dose dependant manner, *Leuk. Res.*, 2016, **51**, 56–61.
- 23 A. Smith, B. Giunta, P. C. Bickford, M. Fountain, J. Tan and R. D. Shytie, Nanolipidic particles improve the bioavailability and alpha-secretase inducing ability of epigallocatechin-3-gallate (EGCG) for the treatment of Alzheimer's disease, *Int. J. Pharm.*, 2010, **389**(1–2), 207–212.
- 24 Z. Chen, C. Wang, J. Chen and X. Li, Biocompatible, functional spheres based on oxidative coupling assembly of green tea polyphenols, *J. Am. Chem. Soc.*, 2013, **135**(11), 4179–4182.
- 25 J. Li, S. Wu, C. Wu, L. Qiu, G. Zhu, C. Cui, Y. Liu, W. Hou, Y. Wang, L. Zhang, I. T. Teng, H. H. Yang and W. Tan, Versatile surface engineering of porous nanomaterials with bioinspired polyphenol coatings for targeted and controlled drug delivery, *Nanoscale*, 2016, **8**(16), 8600–8606.
- 26 H. Zhang, Z. Yi, Z. Sun, X. Ma and X. Li, Functional nanoparticles of tea polyphenols for doxorubicin delivery in cancer treatment, *J. Mater. Chem. B*, 2017, **5**(36), 7622–7631.
- 27 S. Wang, T. Xu, Y. Yang and Z. Shao, Colloidal Stability of Silk Fibroin Nanoparticles Coated with Cationic Polymer for Effective Drug Delivery, *ACS Appl. Mater. Interfaces*, 2015, **7**(38), 21254–21262.
- 28 T. G. Shutava, S. S. Balkundi, P. Vangala, J. J. Steffan, R. L. Bigelow, J. A. Cardelli, D. P. O'Neal and Y. M. Lvov, Layer-by-Layer-Coated Gelatin Nanoparticles as a Vehicle for Delivery of Natural Polyphenols, *ACS Nano*, 2009, **3**, 1877–1885.
- 29 B. Wang, W. Yang, J. McKittrick and M. A. Meyers, Keratin: Structure, mechanical properties, occurrence in biological organisms, and efforts at bioinspiration, *Prog. Mater. Sci.*, 2016, **76**, 229–318.
- 30 S. Xu, L. Sang, Y. Zhang, X. Wang and X. Li, Biological evaluation of human hair keratin scaffolds for skin wound repair and regeneration, *Mater. Sci. Eng., C*, 2013, **33**(2), 648–655.

- 31 Z. Sun, Z. Yi, H. Zhang, X. Ma, W. Su, X. Sun and X. Li, Bio-responsive alginate-keratin composite nanogels with enhanced drug loading efficiency for cancer therapy, *Carbohydr. Polym.*, 2017, **175**, 159–169.
- 32 J. Kennedy-Darling and L. M. Smith, Measuring the formaldehyde Protein-DNA cross-link reversal rate, *Anal. Chem.*, 2014, **86**(12), 5678–5681.
- 33 T. Takano, T. Murakami, H. Kamitakahara and F. Nakatsubo, Mechanism of formaldehyde adsorption of (+)-catechin, *J. Wood Sci.*, 2008, **54**(4), 329–331.
- 34 T. Mori, T. Ishii, M. Akagawa, Y. Nakamura and T. Nakayama, Covalent binding of tea catechins to protein thiols: the relationship between stability and electrophilic reactivity, *Biosci. Biotechnol., Biochem.*, 2010, **74**(12), 2451–2456.
- 35 E. Wojciechowska, A. Włochowicza and W. Birczyńska, Application of Fourier-transform infrared and Raman spectroscopy to study degradation of the wool fiber keratin, *J. Mol. Struct.*, 1999, **511**, 307–318.
- 36 M. Can, E. Bulut and M. Özacar, Synthesis and Characterization of Pyrogallol-Formaldehyde Nano Resin and Its Usage as an Adsorbent, *J. Chem. Eng. Data*, 2012, **57**(10), 2710–2717.
- 37 H. Schulz and M. Baranska, Identification and quantification of valuable plant substances by IR and Raman spectroscopy, *Vib. Spectrosc.*, 2007, **43**(1), 13–25.
- 38 O. Vittorio, M. Brandl, G. Cirillo, K. Kimpton, E. Hinde, K. Gaus, E. Yee, N. Kumar, H. Duong, C. Fleming, M. Haber, M. Norris, C. Boyer and M. Kavallaris, Dextran-Catechin_An anticancer chemically-modified natural compound targeting copper that attenuates neuroblastoma growth, *Oncotarget*, 2016, **7**(30), 47479–49493.
- 39 S. Oliver, D. S. Thomas, M. Kavallaris, O. Vittorio and C. Boyer, Efficient functionalisation of dextran-aldehyde with catechin: potential applications in the treatment of cancer, *Polym. Chem.*, 2016, **7**(14), 2542–2552.
- 40 W. Li, M. Yalcin, Q. Lin, M. M. Ardawi and S. A. Mousa, Self-assembly of green tea catechin derivatives in nanoparticles for oral lycopene delivery, *J. Controlled Release*, 2017, **248**, 117–124.
- 41 K. Lu, W. Ye, L. Zhou, L. B. Collins, X. C. Gold, L. M. Ball and J. A. Swenberg, Structural Characterization of Formaldehyde-Induced Cross-Links Between Amino Acids and Deoxynucleosides and Their Oligomers, *J. Am. Chem. Soc.*, 2010, **132**, 3388–3399.
- 42 K. J. Siebert, N. V. Troukhanova and P. Y. Lynn, Nature of Polyphenol-Protein Interactions, *J. Agric. Food Chem.*, 1996, **44**, 80–85.
- 43 Q. Li, L. Zhu, R. Liu, D. Huang, X. Jin, N. Che, Z. Li, X. Qu, H. Kang and Y. Huang, Biological stimuli responsive drug carriers based on keratin for triggerable drug delivery, *J. Mater. Chem.*, 2012, **22**(37), 19964.
- 44 O. Tredan, C. M. Galmarini, K. Patel and I. F. Tannock, Drug resistance and the solid tumor microenvironment, *J. Natl. Cancer Inst.*, 2007, **99**(19), 1441–1454.
- 45 H. Zhang, J. Fei, X. Yan, A. Wang and J. Li, Enzyme-Responsive Release of Doxorubicin from Monodisperse Dipeptide-Based Nanocarriers for Highly Efficient Cancer Treatment In Vitro, *Adv. Funct. Mater.*, 2015, **25**(8), 1193–1204.
- 46 L. C. Tsai, H. Hsieh, K. Y. Lu, S. Y. Wang and F. L. Mi, EGCG gelatin-doxorubicin gold nanoparticles enhance therapeutic efficacy of doxorubicin for prostate cancer treatment, *Nanomedicine*, 2016, **11**, 9–30.